A Multiphase Model for pulsed ns-Laser Ablation of Copper in an ambient Gas

D. Autrique*, Z. Chen†, V. Alexiades**, A. Bogaerts† and B. Rethfeld*

*Department of Physics and Optimas Research Center, TU Kaiserslautern, 67653 Kaiserslautern, Germany
† University of Antwerp, 2610 Wilrijk, Belgium
** University of Tennessee Knoxville, 37996-1300 Tennessee, USA

Abstract. Laser ablation in an ambient gas is nowadays used in a growing number of applications, such as chemical analysis and pulsed laser deposition. Despite the many applications, the technique is still poorly understood. Therefore models describing the material evolution in time during short pulse laser irradiation can be helpful to unravel the puzzle and finally result in the optimization of the related applications. In the present work, a copper target is immersed in helium, initially set at atmospheric pressure and room temperature. Calculations are performed for a Gaussian-shaped laser pulse with a wavelength of 532 nm, full width at half maximum of 6 ns, and laser fluences up to 10 J/cm^2.In order to describe the transient behaviour in and above the copper target, hydrodynamic equations are solved. An internal energy method accounting for pressure relaxation is applied for the description of the target. In the plume domain a set of conservation equations is solved,assuming local thermodynamic equilibrium. Calculated crater depths and transmission profiles are compared with experimental results and similar trends are found. Our calculations indicate that for the laser fluence regime under study, explosive boiling could play a fundamental role in the plasma formation of metals under ns-pulsed laser irradiation.

Keywords: nanosecond, laser ablation, background gas, hydrodynamics, multiphase, explosive boiling
PACS: 44.10,47.10.ad,52.25Jm,52.52Os
email:dautriqu@physik.uni-kl.de

INTRODUCTION

The interaction of laser light with solid targets and the properties of laser-produced plasmas have been investigated for many years. Several analytical methods apply the technique of laser-solid interaction, under different laser conditions, such as matrix assisted laser desorption ionization (MALDI) [1, 4], laser microprobe mass spectrometry (LMMS) [2], laser induced breakdown spectrometry (LIBS) [3] as well as laser ablation (LA) [4]. The latter is used in a growing number of applications. Several material processing techniques apply the ablation processes in an ambient environment. During pulsed laser deposition for instance, the insertion of a background gas reduces the ablated plume energy considerably and allows one to vary the film thickness [5]. Direct solid microanalysis using laser ablation in combination with inductively coupled plasma mass spectrometry (LA-ICP-MS) is a frequently used technique for fast and powerful multi-element determination of solid samples at the trace and ultra-trace concentration levels for a variety of sample types [6, 7]. Here the ambient gas is used to transport the ablated matter towards the analysis equipment.

Despite the large number of scientific and practical applications of laser ablation, the technique is still poorly understood. Laser-material interaction results in many complicated physical

processes, which depend on the thermo-physical properties of the sample, the laser characteristics, as well as the ambient environment. Besides, the experimental conditions often complicate the identification of the underlying mechanisms. Since theoretical models allow a separate study of the various processes, they are a complementary tool during the research quest. Moreover they can also help to optimize the above-mentioned applications.

At present, various models are applied to study the transient behavior in and above the target [8-28]. In the past decade a large number of hydrocodes has been developed for the study of ns-pulsed laser ablation of metals [8-28]. Their popularity stems from the fact that they don't suffer from severe time- and length-scale limitations, contrary to kinetic models [8-13]. Among the present hydrodynamic models for pulsed ns-laser ablation one can distinguish models that are spatially one-, two- and three-dimensional; models accounting for target heating; models dealing with plasma formation; models that consider ablation in an ambient environment and/or a combination of these features.

Nevertheless, several hydrocodes suffer from serious constraints with respect to their target treatment. In a lot of cases, surface evaporation is considered as the dominant mass removal mechanism [19-28]. Surface evaporation is characterized by a clear phase boundary between the liquid and vapor phases and a transient non-equilibrium layer adjacent to the boundary denoted as the Knudsen layer [29, 30].

Typically authors apply here the Clausius-Clapeyron-equation to calculate the binodal properties [19-28]. In principle these models can only be applied in a limited fluence regime, approximately $F < 1$ GW/m^2 [29, 30]. At higher laser intensities the metal reaches temperatures near the critical temperature.

As a result a clear phase boundary cannot be distinguished anymore and the target treatment has to be revised. A lot of interesting work has been performed to circumvent this problem. In several cases the laser fluence was chosen in such a way that the material did not exceed its critical temperature [20-25]. Other authors accounted for variable optical properties. According to the work of Batanov [31] and Karapetyan [32], for instance, some authors assumed that the liquid metal transforms into a transparent dielectric near the critical temperature [14, 26, 27]. This idea is quite attractive from both a computational as well as a physical point of view, since one can still attach an evaporation front to the hot metal, i.e. the binodal properties can be considered at all times.

Nevertheless,we will demonstrate below that such a model results in serious deviations from the experiment. There are two important drawbacks of these models: in principle the dielectric layer should be treated as a *quasi-transparent* layer and besides, such regarded models would not allow for *phase explosion* [33]. During the latter process, the target reaches temperatures nearby 0.9 T_C. Here, homogenous nucleation triggers bubble growth in the liquid layer and results in explosive boiling: the superheated liquid is converted into a mixture of vapor and liquid droplets.

After phase explosion was introduced in the field by Martynyuk [34, 35], it was identified as a potential mass removal mechanism for laser ablation and therefore thoroughly investigated [14, 36-43]. An excellent overview treating this subject has been written by N.A. Bulgakova and A.V. Bulgakov [38].

In this manuscript a 1D-multiphase model is presented that accounts for target heating, evaporation, explosive boiling as well as plume expansion and plasma formation under ns-pulsed laser ablation in an ambient environment.

A copper target is immersed in helium, initially set at atmospheric pressure and room temperature. Calculations are performed for a laser pulse with a wavelength of 532 nm, full width at half maximum of 6 ns, and laser fluences up to 10 J/cm^2. The results are compared with experimental data [28, 41]. In the next section, the main aspects of the model are presented. Due to

the large dataset, a detailed discussion and tabulation of the applied material properties is out of the scope of this manuscript and planned for future work. Instead the readers are provided with the key references from which the parameters were retrieved. Here we focus on a detailed model description as well as the discussion of the obtained results.

MODEL

Melting and Evaporation

During the initial stage of ns-laser ablation of metals, a part of the laser energy is absorbed by the material, near the sample surface. The absorbed energy is subsequently transferred by heat conduction further into the interior of the target, followed by melting and evaporation. Finally the evaporated material expands above the target and eventually ionizes, resulting in a dense plasma which shields the target from the laser beam.

For ns-laser irradiation, one can assume that the laser energy absorbed by the electrons is instantaneously redistributed and passed to the lattice [44]. Therefore, target heating can be described by a heat conduction equation. The appropriate conservative variable, one solves for, is the internal energy density [45]. Since the material evaporates, it can be described in a reference frame attached to the receding surface. The resulting equation is:

$$\frac{\partial U(t,z)}{\partial t} - v_{rec}(t)\frac{\partial U(t,z)}{\partial z} = \frac{\partial}{\partial z}\kappa(T)\frac{\partial T(t,z)}{\partial z} + S_{las}(t,z) \tag{1}$$

$$S_{las}(t,z) = (1-R(T))\alpha(T)I(t)\exp(-\alpha(T)z) \tag{2}$$

In Eq.(1), U denotes the internal energy density, v_{rec} is the surface recession velocity, κ is the thermal conductivity and S_{las} the laser source term. The latter can be reconstructed by applying the Lambert-Beer law; the result is given by Eq.(2). The source term is composed of the reflectivity R, absorption coefficient α and the impinging laser intensity I.

The temperature dependent thermal conductivity for copper is retrieved from [46]. The optical properties R and α depend on the applied laser wavelength as well as the temperature of the material. They are calculated by fitting the extended Drude model described in [47] to tabulated data [48] and applying the Wiedemann Franz-law. The resulting figures can be found in Section 3.

Since the material is heated to high temperatures, the thermophysical properties of the material change significantly. Therefore an equation-of-state table was inserted in the model [49].

Note that the laser heated material tends to achieve equilibrium with its ambient pressure. Since the mechanical relaxation time for laser irradiated metals is in the order of picoseconds [50], this process can therefore be regarded as an instantaneous event.

Accordingly, the temperature can be retrieved by the following closure relation:

$$U = \rho u \tag{3}$$

$$u = u(T,\rho,P_m) \tag{4}$$

Here u,ρ,P_m denote the specific internal energy, mass density and material pressure, respectively.

Knudsen Layer

Above the target, the evaporated particles achieve translational equilibrium within a few mean free path lengths, by means of collisions. This transition layer is known as the Knudsen layer (KL). The Knudsen layer provides the connection between the 'inner world' (target) and the 'outer world' (plasma plume). Across the Knudsen Layer, treated as a gas dynamic discontinuity, conservation of mass, momentum and energy impose certain jump conditions on temperature, pressure, density, and velocity.

There exists extensive literature on Knudsen layer modeling, at various scales and levels of detail [51-57]. A useful treatment was given by Knight [52], whose relations account for evaporation into a background gas.

$$\frac{T_K}{T_S} = \left[\sqrt{1+\pi\left(\frac{m}{2}\left(\frac{\gamma-1}{\gamma+1}\right)\right)^2} - \sqrt{\pi}\frac{m}{2}\left(\frac{\gamma-1}{\gamma+1}\right) \right]^2 \tag{5}$$

$$\frac{P_K}{P_S} = \sqrt{\frac{T_K}{T_S}}\left[\left(m^2+\frac{1}{2}\right)e^{m^2}erfc(m) - \frac{m}{\sqrt{\pi}}\right] + \frac{1}{2}\left[1-\sqrt{\pi}e^{m^2}erfc(m)\right] \leq 1 \tag{6}$$

$$with\ m = \frac{u_K}{\sqrt{2RT_K}},\ M = u_K\sqrt{\frac{2}{\gamma}} \tag{7}$$

Here P_S and T_S denote the surface pressure and temperature, whereas P_K and T_K are the pressure and temperature at the outer side of the Knudsen layer. γ is the specific heat ratio. The particles that leave the surface achieve a bulk velocity after several collisions; the corresponding speed ratio and Mach number are expressed by m and M, respectively. The present relations account only for evaporation; accordingly the pressure ratio given in Eq.(6), is always less than one.

In a plasma, high pressures can be built up; therefore, one has to account for condensation as well. In this scenario, a pressure ratio exceeding one and a negative Mach number are found ($P_K/P_S > 1$, $M < 0$). Contrary to evaporation, condensation can be subsonic, as well as supersonic [57]. In the supersonic case all variables are extrapolated, whereas in the subsonic case the following pressure ratio is applied [58]:

$$P_K/P_S = 0.95e^{(2.42|M|)}. \tag{8}$$

Boundary conditions

The Knudsen layer results in the following boundary conditions:

$$F_\rho = \rho_K u_K \tag{9}$$

$$F_{\rho u} = \rho_K u_K^2 + P_K \tag{10}$$

$$F_{\rho\varepsilon} = (\rho_K \varepsilon_K + P_K)\, u_K \tag{11}$$

Eq.(9), Eq.(10) and Eq.(11) denote the mass, momentum and energy flux, respectively. ρ_K and ε_K are the mass density and the specific total energy at the outer side of the Knudsen layer, respectively. Finally the heat flux Q_K between the target and plume domain is estimated by means of its mean free path $\lambda_K = 1/n_K\sigma_K$ as $Q_K = (T_S - T_K)/\lambda_K$. Here n_K and σ_K are the number density of the vapor species and the momentum transfer cross section, respectively. The momentum cross section is in the order of $10^{-18}\mathrm{m}^2$ [59].

Explosive boiling

As mentioned above, the present model accounts for phase explosion, i.e. explosive boiling. As soon as temperatures around 0.9 T_C are reached, large fluctuations in density and entropy appear. The hot liquid metal arrives in a metastable state between the binodal and the spinodal of the phase diagram [36-38, 42]. Here explosive boiling tends to drive the system into a new equilibrium state. A fast increase of the homogenous nucleation rate, followed by bubble growth, results in the ejection of a mixture of vapor and liquid droplets. Experiments as well as simulations indicate that this process can happen on the ns- [36, 38, 40] and even on the ps- time scale [38,39]. The homogenous nucleation rate J_c can be derived, by applying the Volmer-Döring theory [60]:

$$J_c = Cn_l(T)e^{-W_c/kT} \tag{12}$$

Here C is a prefactor in the order of $10^8 \mathrm{s}^{-1}$ [58], n_l is the liquid number density and W_c is the work needed to create a nucleus of a critical radius R_{cr} against a surface tension σ. The surface tension vanishes at the critical point, and can be described by applying the extended Eötvös rule [42]:

$$\sigma(T) = \sigma_M \frac{(T_c - T)}{(T_c - T_m)} \left(\frac{\rho_{l,b}(T) - \rho_{g,b}(T)}{\rho_{l,b}(T_m) - \rho_{g,b}(T_m)} \right)^{2/3} \left(\frac{\rho_l(T,P_L) - \rho_{l,sp}(T)}{\rho_{l,sp}(T_m) - \rho_{l,sp}(T_m)} \right)^{2/3} \tag{13}$$

$\rho_{l,b}$ and $\rho_{g,b}$ denote the mass densities on the liquid and gas parts of the binodal, whereas the mass density on the liquid branch of the spinodal is given by $\rho_{l,sp}$. The melting point of copper is denoted as $T_m = 1358\mathrm{K}$, the critical point as $T_c = 8000\mathrm{K}$. $\sigma_M = 1.29\mathrm{J/m}^2$, is the surface tension of copper taken at the melting point [61]. The work term W_c and the critical radius R_{cr} are given by:

$$W_c = \frac{4\pi}{3} R_{cr}^2 \sigma(T) \tag{14}$$

$$R_{cr} = 2\sigma(T) / \left(P_S(T) - P_L(T,\rho)\right) \tag{15}$$

Note that the critical radius is governed by the pressure difference along the bubble surface, Eq.(15). The inner pressure is set here to the binodal pressure P_S at the considered temperature, whereas the outer pressure is set to the pressure P_L . Since our calculations show that the material tends to relax to the ambient pressure, this simply implies that $P_L \cong P_K$. Here P_K is the pressure at the outer side of the Knudsen layer. As a result we find that the pressure ratio P_K/P_S does not only govern surface evaporation, but also influences the volumetric mass removal. This observation is important, since it indicates that explosive boiling does not necessarily proceed continuously. Indeed, in case a high pressure is built up in the ambient environment, the process stops automatically.

Solution procedure

The target domain was discretized into a uniform grid, with a minimum cell size of 5 nm. Eq.(1) is solved explicitely using variable time stepping. The temperatures and corresponding densities were obtained from the equation-of-state tables (see Eqs.(3-4)). In a next step the remaining thermophysical, optical properties as well as boundary conditions are updated. As soon as the target reaches temperatures around 0.9 T_C, explosive boiling starts. In case the nuclei fill a computational cell, the related cell is added to the plume domain and the target surface is repositioned. As a consequence the surface temperature never exceeds T_c, whereas the ejected mass still continues its journey through the phase diagram.

Plume dynamics and plasma formation

Evaporation as well as explosive boiling results in a dense plume, expanding above the copper surface in the ambient environment, which consists of helium. Therefore plume expansion is described by the Navier-Stokes equations for a binary mixture:

$$\frac{\partial \rho}{\partial t} = -\frac{\partial \rho v}{\partial x} \tag{16}$$

$$\frac{\partial \rho_v}{\partial t} = -\frac{\partial \rho_v v}{\partial x} - \frac{\partial}{\partial x} j_m^x \tag{17}$$

$$\frac{\partial \rho v}{\partial t} = -\frac{\partial}{\partial x}\left(\rho v^2 + P + \frac{\partial}{\partial x}\tau_{xx}\right) \tag{18}$$

$$\frac{\partial \rho \varepsilon}{\partial t} = -\frac{\partial}{\partial x}\left[\rho \varepsilon v + P v\right] - \frac{\partial}{\partial x}\left(q + \tau_{xx}\right) + S_{\mathrm{IB}} + S_{\mathrm{MPI}} - S_{rad} \tag{19}$$

The Navier-Stokes equations express mass (Eq. 16), momentum (Eq. 18) and energy conservation (Eq. 19) in the plume domain. Here ρ denotes the total mass density, which is equal to $\rho_v + \rho_b$. ρ_v and ρ_b are the partial densities of the vapor and the background gas. The total momentum density and the total energy density are given by ρv and $\rho \varepsilon$ respectively; P is total pressure. The model accounts for mass diffusion as well as the viscous forces. Here j_m^x represents the mass diffusion flux according to Fick's first law, τ_{xx} is the x-component of the viscosity tensor and q denotes the sum of the conductive and diffusive energy fluxes [62].

In the energy equation one can distinguish three main source terms. S_{IB} and S_{MPI} are the energy source terms due to inverse Bremsstrahlung (IB) and multi-photon ionization (MPI). S_{rad} is the radiation power loss emitted during inverse Bremsstrahlung [63].

The populations of the species can be derived from the principles of equipartition, provided that the plasma conditions do not change too rapidly. As a consequence the species abundances can be recovered through the Saha-Eggert and the Boltzmann relations [63].

The Saha-Eggert equation for an ion in a state i is [63]:

$$\frac{n_e x_i}{x_{i-1}} = \frac{u_i(T)}{u_{i-1}(T)}\left(\frac{2\pi m_e k T}{h^2}\right)^{\frac{3}{2}} \exp\left(-\frac{I_i}{kT}\right) \tag{20}$$

Here n_e is the total electron number density of the two-component mixture, x_i x_{i-1} are the molar fractions of the ions at states i and $i-1$, respectively. I_i is the ionization potential of the ion with respect to state $i-1$, $u_i(T)$ is the electronic partition function for an ion in state i. The required spectroscopic data for the Saha equations were retrieved from the NIST database [64]. Since the maximum fluence is 10 J/cm^2, it is reasonable to limit the number of oxidation states. In the present work the energy levels were limited to the ground states of Cu^{2+} and He^{+} respectively. An approximate Riemann solver is used to solve the hyperbolic set of equations [65], whereas adaptive mesh refinement is used to resolve the gradients of the variables in the computational domain [66]. The Saha equations and corresponding closure relations were solved iteratively by a Newton-Raphson method to calculate the unknowns $x_{e,v}$, $x_{e,b}$, x_i and T.

RESULTS

The model described above is applied for a copper target, immersed in helium. The initial pressure and temperature of both materials correspond to the atmospheric pressure (P=101325 Pa) and room temperature (T=300 K). Calculations are performed for a Gaussian-shaped laser pulse with a wavelength of 532 nm, full width at half maximum (FWHM) of 6 ns, and laser fluences up to 10 J/cm^2. The temporal and spatial behavior of the various physical mechanisms is shown here for a laser operating at a peak intensity of 1.4×10^{13} W/m^2, which corresponds to a total fluence of approximately 9 J/cm^2.

Target

The time evolution of the surface temperature, as well as of the original and actual impinging laser intensities at the target surface, is shown in Fig. 1(a). During the laser pulse the target heats up very fast; after 6 ns the surface cells start to melt (T_m = 1358 K); around 7 ns the surface temperature exceeds the normal boiling point (T_b = 2836 K) and evaporation becomes significant. When the surface reaches temperatures near the critical temperature (T_c = 8000 K), homogenous nucleation becomes important and the liquid metal becomes quasi-transparent. Here a strong reduction of the electron density in the liquid results in a drastic change of the optical properties.

Indeed, the reflectivity starts to drop quickly as shown in Fig. 1(b). As a result the laser light pentrates deep into the material. As a result a thick molten region is formed. Fig. 1(c-d) show the situation in the target near the end of the laser pulse. In the high temperature zone, the conductivity and the mass density decrease significantly. This simply illustrates that the popular *Ansatz* of constant thermophysical properties is quite unrealistic at these laser conditions, and the assumption becomes significantly worse when reaching the critical point.

As the incident laser energy penetrates through this quasi-transparent layer to the underlying material, the transparency front starts to propagate into the interior liquid. Explosive boiling results in a systematic ejection of a dense mixture of liquid and vapor. Alternating advection and compression of matter cause ripples in the Mach number and the pressure ratio, as is shown in Fig. 2. Finally note that due to surface repositioning, the target never exceeds its critical temperature as one can clearly see in Fig. 1.

During the laser action, multi-photon ionization results in the creation of ions and electrons in the dense material plume. These electrons absorb additional energy during inverse Bremsstrahlung processes; they speed up in the laser field and collide with neutrals and ions. This induces an avalanche effect that keeps on increasing the plume temperatures to a few 10000 K: a plasma is created.

At a certain moment, here around 10 ns, the plasma is so dense that it completely shields the target, as depicted in Fig. 1(a). As a result, the surface pressure and temperature decrease, the pressure ratio exceeds 1 ($P_K > P_S > 1$), the Mach number becomes negative, see Fig. 2. This means that condensation starts. At the same moment, the mass density above the target decreases due to advection. Laser light reaches again the target surface, raising the surface temperature and pressure again. Accordingly, the laser intensity profile at the target adapts to a bimodal shape as depicted in Fig. 1(a). At the end of the laser pulse, the amount of laser energy deposited in the plume decreases, the surface temperature and pressure continue to decrease and material keeps on condensing on the surface.

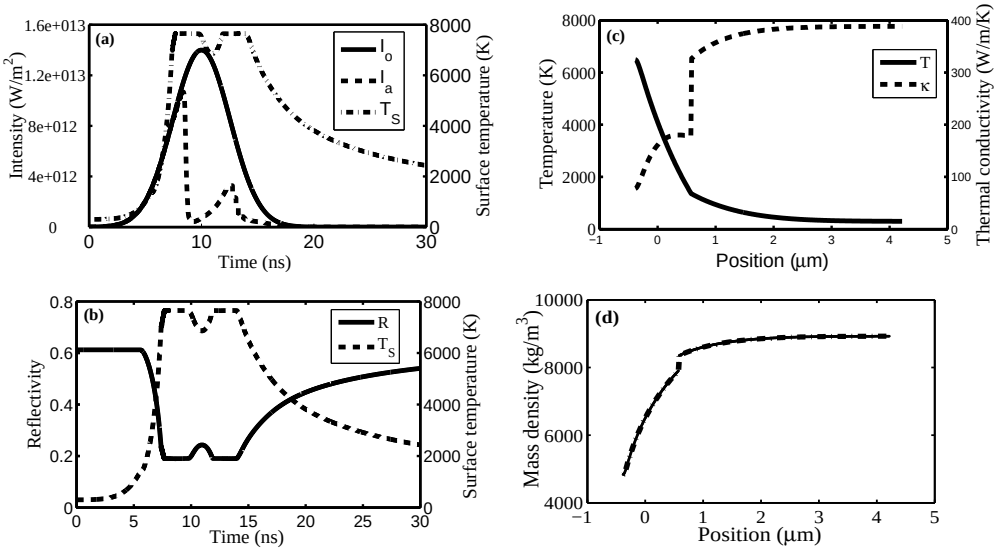

FIGURE 1. (a) Temporal profile of the original laser irradiance I_o, the actual laser irradiance I_a arriving at the target surface, and the target surface temperature T_S. (b) Temporal evolution of reflectivity R, together with target surface temperature. (c) Spatial distribution of the target temperature T and the thermal conductivity at 15 ns. (d) Spatial distribution of the target mass density at 15 ns.

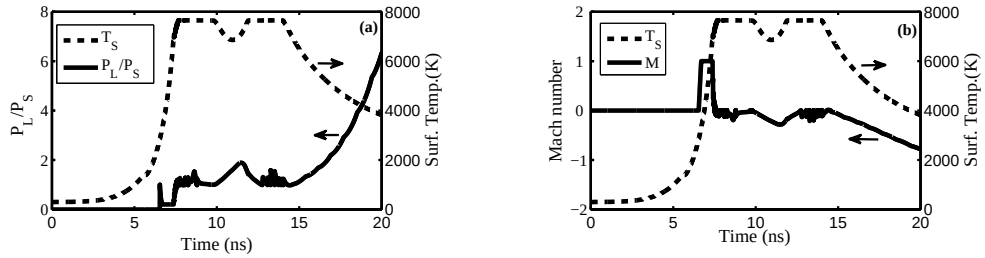

FIGURE 2. (a) Temporal evolution of the pressure ratio P_L/P_S and surface temperature T_S. (b) Temporal evolution of the Mach number M and surface temperature T_S.

Plasma Plume

When the target surface temperature exceeds the boiling point during the laser ablation, copper vapor starts to evaporate from the target and moves away from the surface rapidly. After a while, explosive boiling starts and photo-ionization and inverse Bremsstrahlung processes induce plasma formation in the dense plume. The hot vapor expands above the target and attains large speeds on the order of 10 km/s. This can be clearly seen in Fig. 3(a-b). Finally the temperature and velocity will decrease during the expansion process.

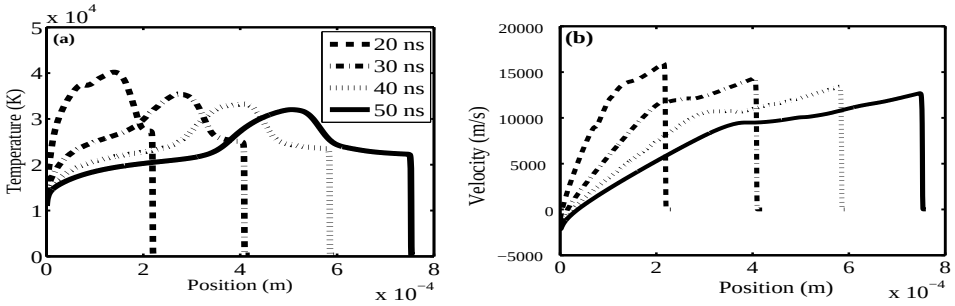

FIGURE 3. (a) Spatial profile of the plume temperature after 20, 30, 40 and 50 ns. (b) Spatial profile of the plume velocity after 20, 30, 40 and 50 ns.

Laser transmission data and crater depths

Crater depths as well as laser transmission data are shown in Fig. 4(a-b) and are crucial for the experimental validation of the model. The model is tested for two situations. In the first situation, we apply the features described above: a quasi-transparent target is considered and matter is removed due to surface as well as volumetric processes. In the second situation, only evaporation is considered. Since we assume a perfect transparent target here, the surface temperature never exceeds the critical point. Therefore an evaporation front can at all times be attached to the surface as was explained in the introduction [14, 26, 27]. As depicted in Fig. 4, pure evaporation results in very large crater depths and no plasma formation: the transmittance is 1. In the second case, the model accounts for explosive boiling. Here plasma formation causes a reduction in the mass removal rate and a drop in the transmittivity. The latter was also observed in [41].

In Refs. [28, 67], experiments were reported for laser ablation of copper in argon [28] and helium [67] under atmospheric pressure. In both cases the laser regime was very similar to the present one. Crater depths up to 85 nm [28, 67] and similar transmissivity data [67] as the calculated ones depicted in Fig. 4(b) were measured. The results indicate that explosive boiling should be considered in order to explain the experimentally observed crater depths as well as the transmission profile.

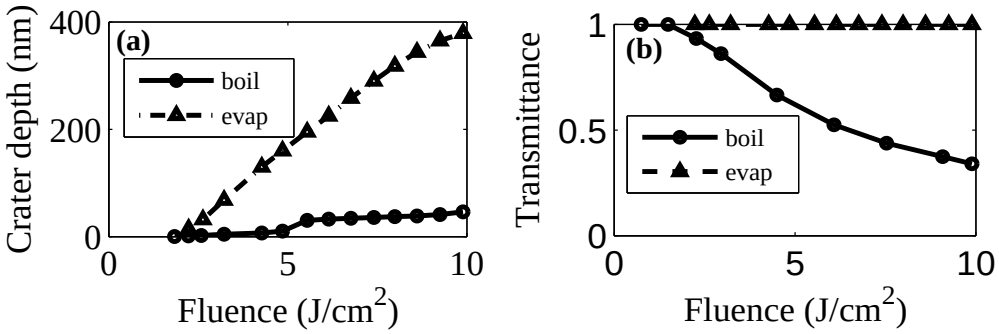

FIGURE 4. (a) Crater depth vs fluence (b) transmittance vs fluence. Model with (boil) and without (evap) explosive boiling.

CONCLUSIONS

A hydrodynamic multiphase model for laser ablation of copper in helium at atmospheric pressure has been presented. During laser irradiation, several complex, tightly coupled physical processes occur in and above the target. At sufficiently high intensities (=1 GW/cm^2) the copper sample reaches temperatures near the critical temperature, resulting in a quasi-transparent metastable liquid layer. Here volumetric mass removal starts. Homogenous nucleation results in bubble growth in the liquid layer, followed by explosive boiling. Subsequently a dense mixture of liquid and vapor is ejected in the plume domain. The dense ejected mass triggers plasma formation. The resulting plasma suppresses further bubble growth and absorbs the incoming laser light. During this stage, the surface temperature drops and vapor recondenses on the target. After the laser pulse, the plume expands further above the target.

The calculated crater depths and transmission data were compared with experimental results and similar trends are found . Our results indicate that explosive boiling can play an important role in the plasma formation of metals under ns-pulsed laser irradiation. It could therefore be regarded as a fundamental mechanism in hydrocodes describing pulsed ns-laser ablation at higher fluences.

ACKNOWLEDGMENTS

The authors wish to thank Prof Dr. N. Bulgakova for her valuable comments and efforts. Dr P. Levashov, Dr. K. Khishenko and Dr. M. Povarnitsyn are deeply acknowledged for their advice and equation-of-state data set. The authors acknowledge financial support from the Deutsche Forschungsgemeinschaft (Emmy Noether-Program, grant RE 1141/11) and the Flemish Fund for Scientific Research (FWO Vlaanderen).

REFERENCES

1. W. Schrepp and H. Pasch, MALDI-TOF Mass Spectrometry of Synthetic Polymers, Berlin:Springer-Verlag, 2003, pp.57-82.
2. E. Denoyer, R. Van Grieken, F. Adams, D.F.S. Natusch, Anal. CHem. **54** (1), 26A (1982).
3. D.A. Cremers, L .J. Radziemski, Handbook of Laser-Induced Breakdown Spectroscopy,Chich:Wiley, 2006,pp.1-50.
4. J. C. Miller, R. F. Haglund, Laser ablation and desorption, NY: Academic Press, 1998, pp. 15-126 and pp. 413-439.
5. D. B. Chrisey and G.K. Hubler, Pulsed Laser Deposition of Thin Films, NY: Wiley, 1994, pp. 184.
6. A. Montaser, Inductively Coupled Plasma Mass Spectrometry, NY: Wiley, 1998, pp. 83-224.
7. J. S. Becker,Spectrochim. Acta Part B **57**, 1805 (2002).
8. I. NoorBatcha, R. R. Lucchese, and Y. Zeiri, J. Chem. Phys. **86**, 5816 (1987).
9. D. Sibold and H. M. Urbassek, J. Appl. Phys. **73**, 8544 (1993).
10. T.Itina, V. N. Tokarev, W. Marine, and M. Autric, J. Chem. Phys. **106**, 8905 (1997).
11. J. C. S. Kools, J. Appl. Phys. **74**, 6401 (1993).
12. F. Garrelie, J. Aubreton, and A. Catherinot, J. Appl. Phys. **83**, 5075 (1998).
13. V. I. Mazhukin, V.V. Nossov, M. G. Nickiforov, and I. Smurov, J. Appl. Phys. **93**, 56 (2003).
14. C. Porneala and D. A. Willis, Int. J. Heat Mass Transfer **49**, 1928 (2006).
15. J. H. Yoo, SH Jeong, R. Greif, R. E. Russo, J. Appl. Phys. **88**, 1638 (2000).
16. A. V. Bulgakov and N. M. Bulgakova, J. Phys. D **28**, 1710 (1995).
17. S.I. Anisimov, B.S. Luk'yanchuk, A. Luches, Appl. Surf. Sci. **96**, 24 (1996).

18. R. F. Wood, K. R. Chen, J. N. Leboeuf, A. A. Puretzky, and D. B. Geohegan,, Phys. Rev. Lett. **79**, 1571 (1997).
19. E. Itina, J. Hermann, Ph. Delaporte, and M. Sentis, Phys. Rev. E **66**, 066406 (2002).
20. M. Aden, E. W. Kreutz, and A. Voss, J. Phys. D **26**, 1545 (1993).
21. J. R. Ho, C. P. Grigoropoulos, and J. A. C. Humphrey, J. Appl. Phys. **78**, 4696 (1995).
22. H. C. Le, D. E. Zeitoun, J. D. Parisse, M. Sentis, W. Marine, Phys.Rev.E **62** (3), 4152 (2000).
23. V. I. Mazhukin, I. Smurov, C. Dupuy, D. Jeandel, Num. Heat Transfer,Part A **26**, 587-600 (1994).
24. A. G. Gnedovets, A. V. Gusarov, and I. Smurov, J. Phys. D **32**, 2162 (1999).
25. Z. Chen and A. Bogaerts, J. Appl. Phys., **97**, 063305 (2005).
26. V. I. Mazhukin, V.V. Nossov and I. Smurov, Appl. Surf Sci, **253**, 7686 (2007).
27. V. I. Mazhukin, V.V. Nossov and I. Smurov, J.Appl. Phys., **101**, 024922 (2007).
28. G. Clair, 'Etudes théorique et expérimentale des plasmas produits par laser en vue de leur application à l'analyse chimique des matériaux en environment complexe', Ph.D. Thesis, Université d'Aix-Marseille II, 2011.
29. M. von Allmen, Laser-Beam Interactions with Materials, Springer, 1987.
30. D. Bäuerle, Laser processing and chemistry, Berlin, Springer Verlag, 2011.
31. V. A. Batanov, F.V. Bunkin, A. M. Prokhorov, and V. Fedorov, Sov. Phys., JETP, **36**, 311 (1973).
32. R. V. Karapetyan and A. A. Samokhin, Sov. J. Quantum Electron., **4**, 1141 (1975).
33. B. Wu and Y.C. Shin, Appl. Phys. Lett , **89**, 111902 (2006).
34. M.M. Martynyuk, Sov. Phys. Tech. Phys.,**19**, 793 (1974).
35. M.M. Martynyuk, Russ. J. Phys.Chem., **57**, 810 (1983).
36. A. Miotello and R. Kelly, Appl. Phys. Lett., **67** (24), 3535 (1995).
37. A. Miotello and R. Kelly, Appl. Phys. A-Mater, **69**, 67 (1999).
38. N. M. Bulgakova and A. V. Bulgakov, Appl. Phys. A-Mater, **73**, 199 (2001).
39. N. Bulgakova and I. Bourakov, Appl. Surf. Sci, **197-198**, 41 (2002).
40. J. Yang, Y. Zhao and X. Zhu. Appl. Phys. Lett., **88**, 094101 (2006).
41. X. Xu, Appl. Surf. Sci., **197-198**, 61 (2002)
42. M. E. Povarnitsyn, P . R. Levashov and K. V. Khishchenko Proceed. of SPIE, **7005**, (2008).
43. M. Povarnitsyn, T. Itina, M. Sentis, K. Khishchenko and P. Levashov, Phys. Rev. B, **75**, 1 (2007).
44. B. N. Chichkov, C. Momma, S. Nolte, F. von Alvensleben and A. Tännermann, Appl. Phys. A-Mater, **63**, 109 (1996).
45. A. V. Bushman, G. I. Kanel', L. A. Ni and V. E. Fortov, Intense Dynamic Loading of Condensed Matter. Washington: Taylor & Francis, pp. 116-145, 1993.
46. C. Y. Ho, R.W. Powell and P.E. Liley, J. Phys. Chem. Ref. Data, **1**, 279 (1972).
47. S. J Youn, T. H. Rho, B. I. Min and K. S. Kim, Phys. Status Solidi B, **244**, 1354 (2007).
48. E. D. Palik, Handbook of Optical Constants of Solids, NY: Academic Press, Vol. 1, pp.280 (1997).
49. P. R. Levashov and K. V. Khishchenko, 'ITTEOS 5.8 software for calculation of EOS for Metals', 2007.
50. B. Chimier, V. T. Tikhonchuk, and L. Hallo, Appl Phys A, **92**, 843-848 (2008).
51. S. I. Anismov, Sov. Phys., JETP, **27**, 182 (1968).
52. C. J. Knight, AIAA Journal, **17**, 519 (1979).
53. C. J. Knight, AIAA Journal, **20**, 950 (1981).
54. A.V. Gusarov and I. Smurov, Phys Fluids, **14**, 4242 (2002).
55. T. Ytrehus, "Theory and experiments on gas kinetics in evaporation", in Rarefied Gas Dynamics, edited by Potter, NY, AIAA, 1977, pp. 1197-1212.
56. A. Miotello, A. Peterlongo, R. Kelly, Nucl Instr. Meth. B, **101**, 148 (1995).
57. I. A. Kuznetsova, A. A. Yushkanov, and Yu. I. Yalamov, High Temp. **38**, 614 (2000).
58. V.I. Mazhukin, V.V. Nossov, I. Smurov, Thin Solid Films, **453-454**, 353 (2004).
59. B. Chervy, O. Dupont, A. Gleizes, and P. Krenek, J. Phys. D, **28**, 2060 (1999).
60. V.P. Skripov, Metastable liquids, NY:Wiley,1973, pp. 1-50.
61. O.Flint, J. Nucl. Mater, **16**, 233 (1965).
62. R. B. Bird, W. E. Stewart, E. N. Lightfoot, Transport Phenomena ,2nd Edition, NY:Wiley, 2006, pp. 1-539.
63. Ya. B. Zel'dovich and Y.P. Raizer, Physics of Shock Waves and High-Temperature Hydrodynamic Phenomena, Vol 1, NY: Dover, 1966, pp.192-292.
64. NIST spectroscopic database at http://www.nist.gov/pml/data/asd.cfm

65. E. F. Toro, M. Spruce, and W. Speares, Shock Waves, **4**, 25 (1994).
66. H.Tang, T.Tang, SIAM J. Numer. Anal, **41**, 487 (2004).
67. Z. Chen, D. Bleiner, A. Bogaerts, J. Appl. Phys. **99**, 063304 (2006).